In-flight thermal experiments for LISA Pathfinder: Simulating temperature noise at the Inertial Sensors

2015 J. Phys.: Conf. Ser. 610 012023

(http://iopscience.iop.org/1742-6596/610/1/012023)

In-flight thermal experiments for LISA Pathfinder: Simulating temperature noise at the Inertial Sensors

F Gibert[a], M Nofrarias[a], M Armano[b], H Audley[c], G Auger[d], J Baird[n], P Binetruy[d], M Born[c], D Bortoluzzi[e], N Brandt[f], A Bursi[t], M Caleno[g], A Cavalleri[h], A Cesarini[h], M Cruise[i], K Danzmann[c], I Diepholz[c], R Dolesi[h], N Dunbar[j], L Ferraioli[k], V Ferroni[h], E Fitzsimons[f], M Freschi[b], J Gallegos[b], C García Marirrodriga[g], R Gerndt[f], Ll Gesa[a], D Giardini[k], R Giusteri[h], C Grimani[l], I Harrison[m], G Heinzel[c], M Hewitson[c], D Hollington[n], M Hueller[h], J Huesler[g], H Inchauspé[d], O Jennrich[g], P Jetzer[o], B Johlander[g], N Karnesis[a], B Kaune[c], N Korsakova[c], C Killow[p], I Lloro[a], R Maarschalkerweerd[m], S Madden[g], P Maghami[s], D Mance[k], V Martín[a], F Martin-Porqueras[b], I Mateos[a], P McNamara[g], J Mendes[m], L Mendes[b], A Moroni[t], S Paczkowski[c], M Perreur-Lloyd[p], A Petiteau[d], P Pivato[h], E Plagnol[d], P Prat[d], U Ragnit[g], J Ramos-Castro[q r], J Reiche[c], J A Romera Perez[g], D Robertson[p], H Rozemeijer[g], G Russano[h], P Sarra[t], A Schleicher[f], J Slutsky[s], C F Sopuerta[a], T Sumner[n], D Texier[b], J Thorpe[s], C Trenkel[j], H B Tu[h], D Vetrugno[h], S Vitale[h], G Wanner[c], H Ward[p], S Waschke[n], P Wass[n], D Wealthy[j], S Wen[h], W Weber[h], A Wittchen[c], C Zanoni[e], T Ziegler[f], P Zweifel[k]

[a] Institut de Ciències de l'Espai (CSIC-IEEC), Campus UAB, Facultat de Ciències, 08193 Bellaterra, Spain
[b] European Space Astronomy Centre, European Space Agency, Villanueva de la Cañada, 28692 Madrid, Spain
[c] Albert-Einstein-Institut, Max-Planck-Institut für Gravitationsphysik und Universität Hannover, 30167 Hannover, Germany
[d] APC UMR7164, Université Paris Diderot, Paris, France
[e] Department of Industrial Engineering, University of Trento, via Sommarive 9, 38123 Trento, and Trento Institute for Fundamental Physics and Application / INFN
[f] Airbus Defence and Space, Claude-Dornier-Strasse, 88090 Immenstaad, Germany
[g] European Space Technology Centre, European Space Agency, Keplerlaan 1, 2200 AG Noordwijk, The Netherlands
[h] Dipartimento di Fisica, Università di Trento and Trento Institute for Fundamental Physics and Application / INFN, 38123 Povo, Trento, Italy
[i] Department of Physics and Astronomy, University of Birmingham, Birmingham, UK
[j] Airbus Defence and Space, Gunnels Wood Road, Stevenage, Hertfordshire, SG1 2AS, UK
[k] Institut für Geophysik, ETH Zürich, Sonneggstrasse 5, CH-8092, Zürich, Switzerland
[l] Istituto di Fisica, Università degli Studi di Urbino/ INFN Urbino (PU), Italy
[m] European Space Operations Centre, European Space Agency, 64293 Darmstadt, Germany
[n] The Blackett Laboratory, Imperial College London, UK
[o] Physik Institut, Universität Zürich, Winterthurerstrasse 190, CH-8057 Zürich, Switzerland
[p] SUPA, Institute for Gravitational Research, School of Physics and Astronomy, University of Glasgow, Glasgow, G12 8QQ, UK

[q] Department d'Enginyeria Electrònica, Universitat Politècnica de Catalunya, 08034 Barcelona, Spain
[r] Institut d'Estudis Espacials de Catalunya (IEEC), C/ Gran Capità 2-4, 08034 Barcelona, Spain
[s] NASA Goddard Space Flight Center, 8800 Greenbelt Road, Greenbelt, MD 20771, USA
[t] CGS S.p.A, Compagnia Generale per lo Spazio, Via Gallarate, 150 - 20151 Milano, Italy

E-mail: gibert@ieec.cat

Abstract. Thermal Diagnostics experiments to be carried out on board LISA Pathfinder (LPF) will yield a detailed characterisation of how temperature fluctuations affect the LTP (LISA Technology Package) instrument performance, a crucial information for future space based gravitational wave detectors as the proposed eLISA. Amongst them, the study of temperature gradient fluctuations around the test masses of the Inertial Sensors will provide as well information regarding the contribution of the Brownian noise, which is expected to limit the LTP sensitivity at frequencies close to 1 mHz during some LTP experiments. In this paper we report on how these kind of Thermal Diagnostics experiments were simulated in the last LPF Simulation Campaign (November, 2013) involving all the LPF Data Analysis team and using an *end-to-end* simulator of the whole spacecraft. Such simulation campaign was conducted under the framework of the preparation for LPF operations.

1. Introduction

LISA Pathfinder (LPF) [1] is a shared ESA/NASA mission to demonstrate the technology for future space-basedspace-based gravitational wave observatories, to be launched along the second half of 2015. LPF aims to prove the feasibility of space-borne gravitational wave observatories, such as eLISA [2], by measuring a residual differential acceleration between free-falling test masses below $3 \times 10^{-14}\,\mathrm{m\,s^{-2}Hz^{-1/2}}$ at 1 mHz. The main instrument on board is the LISA Technology Package (LTP), which includes essentially the two Inertial Sensors with the test masses [4] and the Optical Measurement System [3] that provides the high precision relative distance measurements between the test masses.

The acceleration sensitivity of the LTP along its bandwidth of measurement ($1 - 30$ mHz) is limited at the low edge of the band by actuation noise while, at high frequencies the readout noise sets the limit. Other noise sources like magnetic field fluctuations, test mass random charging or temperature noise have a smaller impact to the sensitivity, but still the LTP needs to be equipped with a diagnostics subsystem to measure and characterise their contribution [5].

In order to characterise those thermal related effects that can have an impact in the instrument sensitivity, the LTP counts with a series of (a) thermistors to provide high precision measurements of temperature fluctuations and (b) heaters to apply controlled heat signals to the system. Specific temperature experiments will be carried out on board in order to characterise the temperature noise perturbations on the LTP performance.

Amongst the different kind of thermal perturbations [6], the LTP is specially sensitive to residual temperature gradient fluctuations on the Electrode Housings (EH) of the Inertial Sensors –the structures that host the test masses (TM) and support the layout of electrodes for electrostatic sensing and actuation. Asymmetric temperature distributions on these parts induce forces and torques on the test masses through three different thermal effects:

(i) The **radiometer effect**, significant in rarefied environments where the particles have a mean free path longer than the cavity dimensions.

(ii) The **radiation pressure**, as a consequence of the radiation emitted by a surface, following the Stefan-Boltzmann Law.

(iii) The temperature-dependent flow of particles emitted by a surface, inducing the asymmetric **outgassing** effect.

Their contribution to the LTP performance has been investigated by means of torsion pendulums [7] and will be measured in-flight through a dedicated thermal experiment. In order to assist the design of the experiment, a State-Space Model (SSM) of the thermal-induced forces and torques has been developed [8, 9] and, in a recent LPF simulation campaign we had the opportunity to test both the experiment simulator and the data analysis tools by integrating it to a global satellite simulator.

In this paper we report the results of such a simulation in the following way: the models for the thermal effects are presented in Section 2, the thermal experiment is described in Section 3, the simulation campaign in Section 4 and the analysis in presented in Section 5. The final discussion is found in Section 6.

2. Thermal effects model

The model implemented is based on the linearised expressions for the different thermal effects showed in Table 1. Each F_{ij} is the force on a surface j by the presence of another surface i at a different temperature. K^{ij} are the coefficients with information on the geometry, visibility conditions and constants. The ΔT_{ij} and T_0 terms represent the temperature difference between surfaces and the absolute temperature respectively, while p is the system pressure. Θ_{OG} is the activation temperature for the outgassing effect. More details of the model can be found in [8].

Table 1. Simplified expressions of the thermal effects [8].

Radiometer effect (RM)	$F^{ij}_{RM} = K^{RM}_{ij}\, p\, T_0^{-1}\, \Delta T_{ij}$
Radiation pressure (RP)	$F^{ij}_{RP} = K^{RP}_{ij}\, T_0^{3}\, \Delta T_{ij}$
Outgassing effect (OG)	$F^{ij}_{OG} = K^{OG}_{ij}\, T_0^{-2}\, e^{-\Theta_{OG}\, T_0^{-1}}\ \Delta T_{ij}$

The system surfaces are discretised in order to allow the calculation of net forces and torques on all the TM axis by computing the different node-to-node contributions. The different coefficients K^{ij}, Θ_{OG} and p are considered constant parameters while ΔT_{ij} and T_0 are simulated by means of a thermal model of the spacecraft.

3. The Electrode Housing thermal experiment

The purpose of the experiments is double: first, to determine the thermal coupling of the temperature gradient fluctuations with the interferometer readouts and, secondly, to disentangle the contribution of the different thermal effects. The relevance of the latter is due to the dependence of the radiometer effect on the pressure, that may allow to estimate the contribution of Brownian noise [10], a pressure-dependent effect expected to be the first noise contributor at the lower edge of the bandwidth –close to 1 mHz– after the actuation noise.

By applying alternate sequences of pulses to Heaters 1 and 2 –see Figure 1– a temperature gradient signal is induced on the x axis. Such a signal is measured by combining the readouts of the different thermistors on the EH walls, as:

$$\Delta T_x = \frac{T_3 + T_4 - T_1 - T_2}{2} \tag{1}$$

The thermal coupling coefficient on the X axis is then defined as

$$\alpha_x = \frac{\mathrm{d}\Delta F_x}{\mathrm{d}\Delta T_x} \tag{2}$$

where the F_x is the x component of the force applied to the test mass. Since the different thermal effects have a different dependence on the absolute temperature, $\alpha_x(T)$ can be used as figure of merit to disentangle the different effects described above. This discrimination is achieved by repeating the same alternate heating sequence at different absolute temperatures.

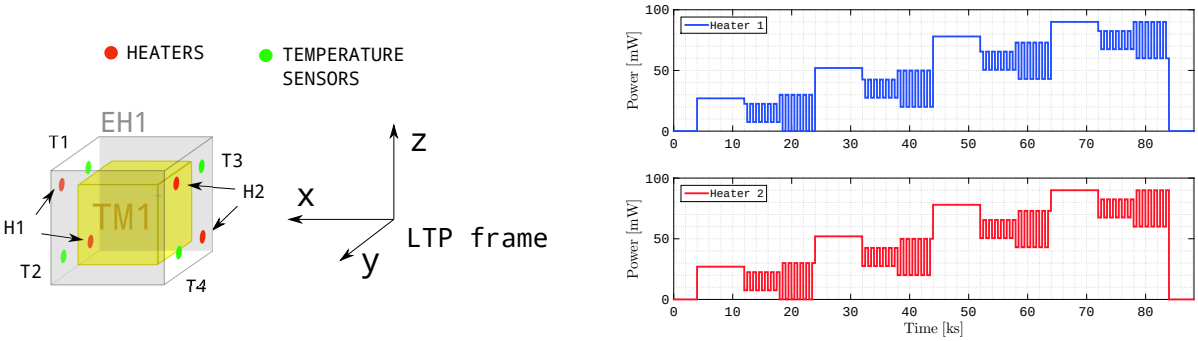

Figure 1. *Left*: Layout of temperature sensors (T1-T4) and heaters (H1, H2) on one of the EH. *Right:* Signals applied to H1 and H2 during the thermal experiment.

4. Simulation campaign

The 4th LPF Simulation Campaign took place in ESAC [1] on November 2013 and lasted for eight days, involving the whole LPF data analysis team. Every day, the telemetry corresponding to the experiments simulated the previous day was received and post-processed and a different group of data analysts was responsible of the analysis. The signal applied to the EH during one day of the campaign consists of the repetition of a same pattern at four different absolute temperature levels, quickly achieved by applying constant voltages to the heaters. At each temperature level, series of pulses of 500 s are applied alternatively to H1 and H2, resulting in a 1 mHz modulated temperature gradient signal along the x axis. For linearity checks, two different modulation amplitudes are applied at each temperature level –see Figure 1.

5. Analysis

The data analysis presented here has been carried out by means of the LTP Data Analysis toolbox, which is a dedicated MATLAB toolbox developed by the LTP scientific community to provide a common working framework during operations [11].

The relevant data for the experiment is presented in Figure 2. A final increment of temperature of 2.5 K is achieved, with the modulation patterns keeping close to stable temperatures. The interferometer response, as expected, is sensitive to the injection only on its differential channel x_{12}, which measures the relative distance between TMs. The control loop that regulates the spacecraft position with respect to the primary TM (x_1) has a high gain at 1 mHz, practically impeding the sensitivity of x_1 to the heat injections, while the control loop on x_{12} actuates on the x axis of the secondary TM with very low gain in the same band.

The temperature gradient signal shows an oscillating pattern with peak-to-peak amplitude levels of 100 and 200 mK as a consequence of the two different modulation amplitudes applied –see Figure 2. The thermal-induced force on the TM is recovered from the telemetry and, as

[1] ESAC: *European Space and Astronomy Centre*, Villanueva de la Cañada, Madrid, Spain

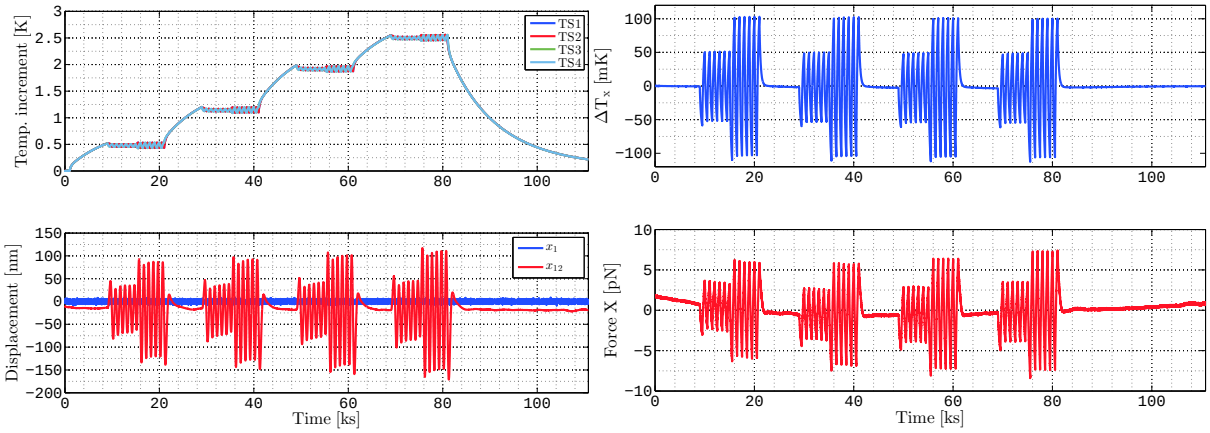

Figure 2. *Top left:* Temperature sensors readouts. *Lower-left* plot: IFO measurements x_1 and x_{12}. *Top right*: Temperature gradient on x axis. *Lower-right* plot: force induced to the TM.

expected, presents the same shape than the temperature gradient signal induced. A delay of about 52 s between the temperature gradient and the force is attributed to intrinsic delays in the thermal model, since the surface nodes used to model the forces are in average geometrically further from the heaters than the thermistors used to measure the temperature gradient.

5.1. Thermal coefficients

The thermal coefficients are obtained by demodulating and dividing the temperature gradient and the force signals. Table 2 show the individual values for each temperature modulation.

Table 2. Thermal coefficients estimated for the different temperature modulations. *A1* and *A2* correspond to the small and large modulation amplitudes respectively.

Temperature [K]	$\alpha_{x,A1}$ [pN/K]	Error [pN/K]	$\alpha_{x,A2}$ [pN/K]	Error [pN/K]
293.48	54.4	0.5	54.4	0.4
294.14	57.8	0.7	57.7	0.6
294.92	62.9	0.7	62.9	0.5
295.50	67.9	0.9	67.9	0.7

The final temperature coefficients are obtained by averaging the values at each temperature level –see Figure 3. The increment with the absolute temperature –much higher than $\propto T^3$– points to an outgassing-dominated scenario. Despite such variation, the reduced increment of absolute temperature available (around 2K between modulation points) limits the identification of the radiometer effect contribution, leaving only the option to set an upper limit of 7.4×10^{-15} m s^{-2} Hz$^{-1/2}$ to the Brownian effect, by considering the worse case of a totally radiometer-dominated environment at the lowest temperature.

5.2. Noise projection to interferometer

In addition to the previous analysis, transfer functions between the temperature gradient and the force can be calculated providing a tool to project the temperature noise to x_{12} equivalent acceleration noise. Figure 3 shows this projection during a specific noise measurement with no thermal injections, showing that the temperature noise to the acceleration sensitivity is kept about a factor 30 below the actual noise level.

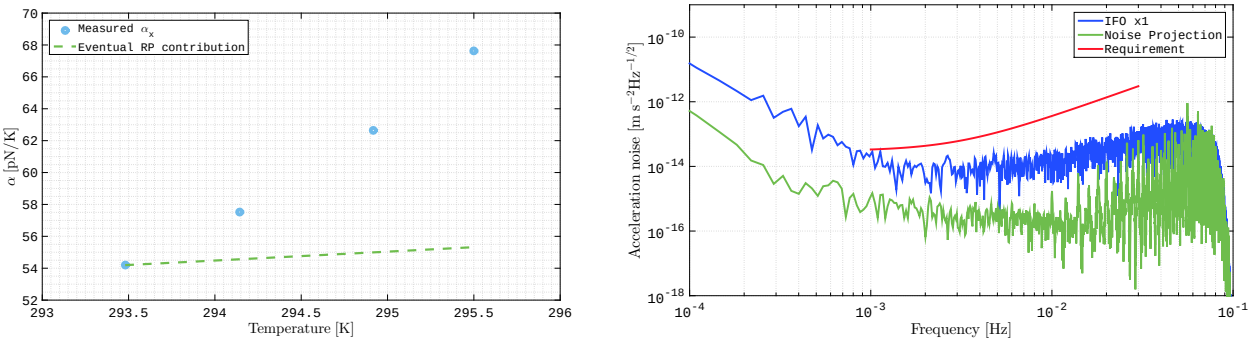

Figure 3. *Left*: Thermal coefficients (α_x) vs. absolute temperature, The comparison of the curve against the third power of the temperature –an eventual dominating radiation pressure contribution at the lowest temperature– suggests an outgassing-dominated scenario. *Right*: Temperature noise projection on an acceleration noise measurement, where the temperature contribution keeps about a factor 30 below the noise level. For $f > 0.02\,\mathrm{mHz}$ the projection is no longer significant since the readout noise of the thermistors is dominant in this band.

6. Discussion

The Electrode Housing thermal experiments to be carried out on board LISA Pathfinder have been simulated and analysed in a dedicated campaign, combining a global spacecraft simulator together with a SSM simulator of the thermal effects. Results show how the current procedure allows to estimate the thermal coefficients with enough precision in an outgassing-dominated environment, but the absolute temperature range is too small to identify the individual contribution of each thermal effect under these circumstances. Even though, an upper limit to the Brownian noise has been obtained from this experiment.

Acknowledgements

The author wants to thank the whole LTP Data Analysis team for the effort in preparing and carrying out the 4th LPF Simulation Campaign. In addition, the author acknowledges support from Project AYA2010-15709 of *Plan Nacional del Espacio* of the Spanish Ministry of Science and Innovation (MICINN).

References

[1] McNamara P *et al* 2013 The LISA Pathfinder Mission, *ASP Conference Series* **467**
[2] Amaro-Seoane P *et al* 2013 The Gravitational Universe, *Document submitted to the European Space Agency for the L2/L3 selection of ESA's Cosmic Vision program*
[3] Heinzel G *et al* 2004 The LTP interferometer and Phasemeter *Class. Quantum Grav.* **21** 581
[4] Dolesi R *et al* 2002 Gravitational sensor for LISA and its technology demonstration mission, *Class. Quantum Grav.* **20** S99
[5] Cañizares P *et al* 2008 The diagnostics subsystem on board LISA Pathfinder and LISA, *Class. Quantum Grav.* **26** 094005
[6] Nofrarias M *et al* 2008 Thermal diagnostic of the Optical Window on board LISA Pathfinder *Class. Quantum Grav.* **24** 5103
[7] Carbone L *et al* 2007, Thermal gradient-induced forces on geodetic reference masses for LISA, *Phys. Rev. D.* **76** 102003
[8] Gibert F *et al* 2012 State-space modelling for heater induced thermal effects on LISA Pathfinder's Test Masses, *J. Phys.: Conf. Ser.* **363** 012044
[9] Gibert F *et al* 2013 Closed Loop Simulations of the Thermal Experiments in LISA Pathfinder, *ASP Conference Series* **467**
[10] Cavalleri A *et al* 2009, Increased Brownian Force Noise from Molecular Impacts in a Constrained Volume, *Phys. Rev. L.* **103** 140601
[11] Hewitson M *et al* 2009 Data analysis for the LISA Technology Package, *Class. Quantum Grav.* **26** 094003